Data Rate Maximization for Terahertz Communication Systems using Finite Alphabets

Anamaria Moldovan[1], Steven Kisseleff[1], Ian F. Akyildiz[2], and Wolfgang H. Gerstacker[1]

[1]Institute for Digital Communications, Friedrich-Alexander-University Erlangen-Nürnberg (FAU), Cauerstr. 7, D-91058 Erlangen, Germany, {anamaria.moldovan, steven.kisseleff, wolfgang.gerstacker}@fau.de
[2]Broadband Wireless Networking Lab, Georgia Institute of Technology, Atlanta, USA, ian.akyildiz@ee.gatech.edu

***Abstract*—With the emergence of numerous novel data-intensive applications, the demand on fast wireless access for huge data file transfer and fast mobile data access is growing rapidly. Following this trend, the "Terabit era" is expected to become a reality in the near future. Terahertz (THz) technology is promising as an enabler due to its unique features, among others such as extremely high bandwidth, resistance to eavesdropping and minimal risk to human health. However, a number of technical hurdles need to be overcome to achieve such ultra-fast data rate of Terabit-per-second (Tbps) in the THz spectrum. In this work, a fundamental insight into the modulation scheme design is aimed to be established for THz communication systems. A strategy for transmission scheme selection and a corresponding efficient power allocation algorithm are proposed. Bounds on the maximum distance are determined for which data rates in the order of Tbps can be achieved. The results provide a fundamental insight into the selection of THz transmission schemes for given performance requirements.**

I. Introduction

Over the last years, the demand for high data rates in wireless communication systems has experienced an unprecedented growth. To satisfy these demands, the network capacity has been enhanced by increasing the spectral efficiency via advanced modulation schemes and signal processing techniques [1]. However, the effects of improving the capacity in this way are limited due to an insufficient bandwidth in current wireless systems, according to Shannon's channel capacity. Beyond this limit, higher operation frequency bands have to be accessed to provide sufficient transmission capacity. According to Edholm's law of bandwidth, the demand for bandwidth in wireless short-range communications has doubled every 18 months over the last 25 years [2]. Extrapolating this growth into the future, much higher wireless transmission rates will be required to support more sophisticated, bandwidth-intensive applications, which will eventually lead to the allocation of wider bandwidths in the Terahertz (THz) frequency range. For this purpose, the IEEE 802.15 Terahertz Interest Group (IGthz) has been established in 2008 to explore the feasibility of the Terahertz band for wireless communications [3]. Since January 2014 there is an official IEEE standardization committee called 100Gbps.

The THz band, or so-called sub-millimeter band, covers the frequency range between 100 GHz and 10 THz, with corresponding free-space wavelengths between 3 mm and 30 μm ("THz gap"). Besides the intrinsic advantage of a higher bandwidth, THz wireless communication links offer some other benefits when compared to microwave or millimeter (mmW) links. THz links are inherently more directional at the same transmitter aperture than mmW links due to the large gain per antenna, which means that beams of THz radiation diffract less during free-space propagation. Consequently, it is possible to minimize the area over which THz radiation can be detected which makes THz suitable for secure communications [4]. Moreover, THz wireless communication links offer some advantages over the infrared (IR) based systems as well, such as lower attenuation of the THz radiation compared to IR links under certain atmospheric conditions (dust, fog) [5] and smaller scintillation effects [6].

Based on these properties, over the past decade, THz waves have become an important tool for selective chemical sensing and bio-medical imaging applications. Yet, the potential use of current existing THz systems is limited by the low output power of THz sources and low sensitivity of THz detectors [7]. In the meantime, however, significant hardware advancements are expected to make THz communications a reality. Gallium Nitride (GaN) based power amplifiers are predicted to generate signals at 1.45 THz at an output power of 2.5 W [8]. Besides, photonic based devices such as quantum cascade laser (QCL) sources, operating in the pulsed mode, exhibit an emission frequency of around 3.4 THz with an output power exceeding 1 W [9]. Recent studies have also proved the existence of technologies for a real time 50 Gbps transmission at 20 m distance [10].

Nevertheless, there still exist many challenges in THz communications requiring innovative solutions, since the well-established technologies may be restricted. Sensitive to atmospheric attenuation due to molecular absorption caused by water vapor and oxygen molecules in the atmosphere, the THz signals experience an extremely severe path loss which limits the communication distance to several tens of meters. Therefore, THz wireless systems will be likely limited to medium-link and short-link indoor applications since outdoor scenarios are much more difficult to handle unless adverse weather conditions are rare [4]. In order to define the indoor THz communication channel, the reflection loss of the typical indoor building materials has to be characterized. In [11] we have proposed a novel deterministic channel model for 0.1 to 1 THz frequency range, based on Kirchhoff scattering theory

978-1-4799-6664-6/16/$31.00 ©2016 IEEE

and ray tracing that includes the effects of line-of-sight (LOS) and non-line-of-sight (NLOS) propagation.

In this work, we investigate digital transmission schemes for THz band systems based on the channel model proposed in [11]. The previous theoretical works mostly consider the channel capacity as a performance measure [11], [12]. However, real methods of digital transmission for THz systems have been only investigated theoretically to a limited extent yet. Consistent with the trend of ultra-low power, pulse-based communication schemes for short range THz communication were proposed in [13]. In [14], a distance-aware multi-carrier modulation scheme which takes advantage of the distance- and frequency-dependent channel peculiarities has been developed. While the mentioned works are mainly on system concepts, there is still room for deeper theoretical investigations that aid the system realization.

Therefore, our proposed scheme takes into the account the effects of inter-symbol interference due to channel dispersion. Thus, we address the performance of the THz band single-carrier transmission in terms of the signal-to-noise ratio per transmitted data symbol at the output of an equalizer. We determine the suitable single-carrier modulation scheme in a channel adaptive fashion, which is still an open issue for THz communication systems. We present an approach based on multiple orthogonal sub-bands to minimize the data rate losses due to modulation schemes with finite-alphabet size by employing an efficient power allocation algorithm. The so-called N-band approach is beneficial for relaxing the requirements on digital-to-analog converters (DACs) and analog-to-digital converters (ADCs), which currently achieve sampling rates up to 100 Gigasamples-per-second [15]. This provides a background for future transceiver design and system adaptation.

This paper is organized as follows. In Section II the system model including the specification of realistic signal filters is provided. In Section III, equalization performance and the suitable modulation scheme selection are addressed. Simulation results are discussed in Section IV. Section V concludes the paper.

II. System Model

The physical mechanisms governing a wireless transmission in the THz band are different from those which affect schemes operating in the lower frequency bands where the propagation is mainly influenced by the spreading loss. Therefore, the implementation of an indoor THz communication link cannot be just an extension of the existing technology. The peculiarities of THz radiation are a very high *molecular absorption* and *spreading loss* which result in a very high and frequency-selective path loss for LOS links. The strong absorption level of atmospheric gases is caused by molecular resonances primarily due to water vapor and oxygen [12]. For NLOS propagation, a very high *reflection loss* depending on the shape, material and roughness of the reflecting surface governs the THz wave propagation [16].

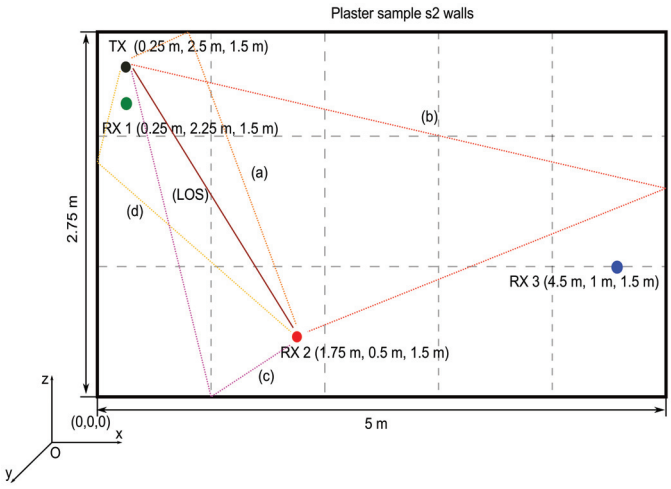

Figure 1: Indoor scenario with three arbitrary TX/RX positions.

A. Channel Modeling

The overall channel transfer function (CTF) is given by [11]

$$H^{\mathrm{OV}}(f,r,\boldsymbol{\zeta}) = H^{\mathrm{LOS}}(f,r)\,\mathrm{e}^{-j2\pi f\tau_{\mathrm{LOS}}} + \sum_{i=1}^{M_{\mathrm{rays}}} H_i^{\mathrm{NLOS}}(f,\zeta_i)\,\mathrm{e}^{-j2\pi f\tau_{\mathrm{NLOS}_i}}, \tag{1}$$

where f is the operation frequency, M_{rays} is the number of indirect rays, $\tau_{\mathrm{LOS}} = r/c$ and $\tau_{\mathrm{NLOS}_i} = \frac{r_{i1}+r_{i2}}{c}$ are the propagation delays of the LOS path and i^{th} NLOS path, respectively, with r denoting the distance between the TX and RX, r_{i1} is the distance between the TX and the i^{th} scattering point and r_{i2} is the distance between the i^{th} scattering point and the RX. The vector $\boldsymbol{\zeta} = [\boldsymbol{\zeta}_1, \ldots, \boldsymbol{\zeta}_{M_{\mathrm{rays}}}]$ describes the coordinates of all scattering points, where $\boldsymbol{\zeta}_i = [r_{i1}, r_{i2}, \theta_{i1}, \theta_{i2}, \theta_{i3}]$ defines the parameters of the i^{th} scattering point location.

The magnitude frequency response of the LOS path $H^{\mathrm{LOS}}(f,r)$ is given by

$$H^{\mathrm{LOS}}(f,r) = H_{\mathrm{spread}}(f,r)\cdot H_{\mathrm{abs}}(f,r), \tag{2}$$

with

$$H_{\mathrm{spread}}(f,r) = \frac{c}{4\pi\cdot f\cdot r}, \tag{3}$$

$$H_{\mathrm{abs}}(f,r) = \mathrm{e}^{-\frac{1}{2}\alpha_{\mathrm{molec}}(f,T_{\mathrm{K}},p)r}, \tag{4}$$

where $c = 2.9979\times 10^8$ m/s is the speed of light, and $\alpha_{\mathrm{molec}}(f,T_{\mathrm{K}},p)$ denotes the total molecular absorption coefficient defined and computed in [12] for a gas at pressure p and temperature T_{K}. The i^{th} NLOS path contribution is defined as

$$H_i^{\mathrm{NLOS}}(f,\zeta_i) = H_{\mathrm{refl},i}(f,r_{i2},\theta_{i1},\theta_{i2},\theta_{i3}) \times H_{\mathrm{spread},i}(f,r_{i1},r_{i2})\cdot H_{\mathrm{abs},i}(f,r_{i1},r_{i2}), \tag{5}$$

with

$$H_{\mathrm{refl},i}(f,r_{i2},\theta_{i1},\theta_{i2},\theta_{i3}) = \sqrt{\mathbb{E}\{R_{\mathrm{power},i}(f,r_{i2},\theta_{i1},\theta_{i2},\theta_{i3})\}}, \tag{6}$$

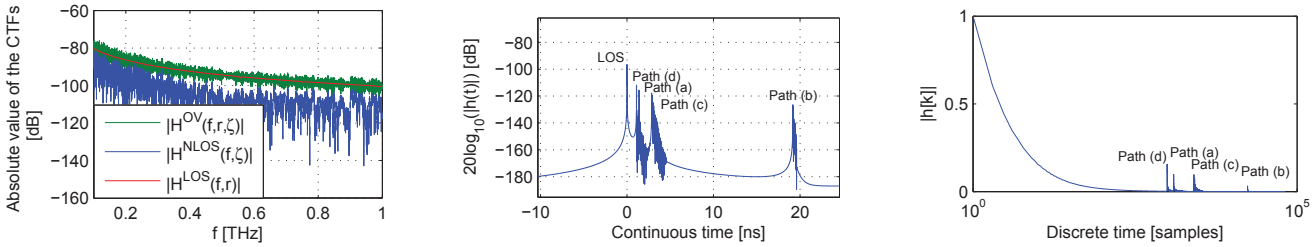

(a) (b) (c)

Figure 2: Transmission channel for TX/RX position 2: (a) magnitude of the CTFs (b) continuous-time impulse response (c) equivalent discrete-time impulse response.

$$H_{\text{spread},i}(f, r_{i1}, r_{i2}) = \frac{c}{4\pi \cdot f \cdot (r_{i1} + r_{i2})}, \tag{7}$$

$$H_{\text{abs},i}(f, r_{i1}, r_{i2}) = \mathrm{e}^{-\frac{1}{2}\alpha_{\text{molec}}(f,T_{\text{K}},p)(r_{i1}+r_{i2})}, \tag{8}$$

where $\mathbb{E}\{R_{\text{power}}(\cdot)\}$ is the average power reflection coefficient of a surface area, describing the scattered power [11].

Our simulation scenario consists of a small rectangular office room (length $\times$ width $\times$ height: $5\ \text{m} \times 2.75\ \text{m} \times 2.5\ \text{m}$), which is visualized in Fig. 1. As an example, we consider TX/RX position 2 (RX labeled in red), i.e., the transmitter is at (0.25 m, 2.5 m, 1.5 m) in the corner of the room, while the receiver is in the same horizontal plane with the transmitter, at (1,75 m, 0.5 m, 1.5m). The LOS and the four specular[1]-reflected rays corresponding to each wall are also depicted. The walls of the room are assumed to be coated with plaster "sample s2" which has a high roughness [16]. Reflections from the floor and from the ceiling are neglected.

The overall CTF highly depends on the geometry of the specific propagation environment, i.e., the position of the TX and RX. In Fig. 2a) the magnitude of the CTFs $H^{\text{LOS}}(f, r)$, $H^{\text{NLOS}}(f, \boldsymbol{\zeta})$ and $H^{\text{OV}}(f, r, \boldsymbol{\zeta})$ for the TX/RX position 2 is depicted. The corresponding impulse response in continuous-time domain shown in Fig. 2b) has been calculated via numerical inverse Fourier transform, $h(t) = \mathcal{F}^{-1}\{H^{\text{OV}}(f, r, \boldsymbol{\zeta})\}$. As observed from Fig. 2b), five main received rays are identified, including the LOS ray and the four specularly reflected rays (a)-(d). Around the delays of the reflected rays in the specular direction, the influence of the non-specular scattering from rough surfaces can be noticed. This effect influences the broadband channel behavior and therefore has been investigated using ray tracing simulations in [11].

B. Noise Modeling

There are two main noise sources in the THz band, namely: molecular absorption noise and thermal noise [17]. The noise power spectral density (PSD) of the molecular absorption noise is given by [12]

$$\Phi_{\text{mol}}(f, r) = k_B T_{\text{mol}}(f, r), \tag{9}$$

where $k_B = 1.3806 \times 10^{-23}$ J/K is the Boltzmann constant and $T_{\text{mol}}(f, r) = T_0(1 - e^{-\alpha_{\text{molec}}(f,T_{\text{K}},p)r})$ denotes the molecular noise temperature with $T_0 = 296$ K being the reference temperature [12]. The thermal noise PSD is given for high frequencies as [18]

$$\Phi_{\text{thermal}}(f) = \frac{\hbar f}{\mathrm{e}^{\frac{\hbar f}{k_B T_0}} - 1}, \tag{10}$$

where $\hbar = 6.6262 \times 10^{-34}$ Js is the Planck's constant.

The total noise power spectral density is obtained as

$$\Phi_{\text{N}}(f, r) = \Phi_{\text{mol}}(f, r) + \Phi_{\text{thermal}}(f). \tag{11}$$

Obviously, the noise in the THz band can no longer be modeled as white. However, the noise coloring can be properly taken into account by signal processing.

C. Signal Filter Design

In order to quantify the performance bounds of the proposed transmission system in the 0.1 to 1 THz range, we use the channel capacity as a metric. Since the channel transfer function $H^{\text{OV}}(f, r, \boldsymbol{\zeta})$ is highly frequency-selective and the PSD of the noise is not flat, the resulting channel capacity can be determined using Shannon's capacity formula for dispersive channels,

$$C(r, \boldsymbol{\zeta}) = \int_B \log_2 \left(1 + \frac{\Phi_{\text{T}}(f, r, \boldsymbol{\zeta})|H^{\text{OV}}(f, r, \boldsymbol{\zeta})|^2}{\Phi_{\text{N}}(f)}\right) \mathrm{d}f, \tag{12}$$

where B is the frequency band from 0.1 to 1 THz used for transmission and $\Phi_{\text{T}}(f_i, r, \boldsymbol{\zeta})$ is the optimum transmit PSD spectrum which corresponds to the waterfilling spectrum and achieves the capacity of the channel limited to band B, $H^{\text{OV}}(f, r, \boldsymbol{\zeta})$ and $\Phi_{\text{N}}(f, r)$ were defined in (1) and (11), respectively. However, for a real system design, the signal generation, reception and processing components need to comply with practical constraints. Hence, the information-theoretical bound given by the Shannon's channel capacity is not an accurate measure for the achievable data rate since transmit pulses assumed to comply with the waterfilling rule can hardly be generated by devices, especially in the THz domain and are not applicable in practice. Instead, a smooth bandlimited waveform (typically a square-root Nyquist filter like a root-raised cosine (RRC) filter) is used for pulse shaping

[1]Specular means that the incident angle θ_1, i.e., the angle between the incident ray and the surface normal equals the reflected angle θ_2, i.e., the angle between the reflected ray and the normal of the surface, and the angle θ_3, defined for scattering directions that lie outside the plane of incidence (x, z) equals to zero.

in practical systems. Moreover, modulation schemes with finite-alphabet size need to be considered.

Since the noise is colored, without any loss of information, a continuous-time noise whitening filter is placed at the first stage of the receiver. Moreover, if the receiver input filter is a matched filter, matched to the cascade representing the equivalent overall channel (transmit filter, channel, continuous-time whitening filter), for a fixed symbol interval T, we may sample without any information loss the continuous-time signal at the rate $1/T$ to obtain a discrete-time model. In our system, $T = \frac{1+\alpha}{B}$, where α is the roll-off factor of the RRC filter and B is the bandwidth of the transmitted waveform. In case of a matched filter, the noise sequence is not white, but colored. Therefore, we employ a whitened matched filter (WMF) before sampling [19]. In this situation, the overall channel becomes minimum-phase and the noise after sampling is white. Since the total discrete-time transmission channel is frequency-selective, an equalization scheme is needed for the signal detection. It is known that a decision-feedback equalization (DFE) scheme with an unbiased minimum mean square error (MMSE) criterion is a canonical receiver structure for ISI channels, i.e., ideal MMSE-DFE (with perfect feedback) is a lossless equalization scheme if used in conjunction with coding [19].

III. Digital transmission scheme

In what follows, we investigate digital transmission strategies for the THz band by addressing the transmission format, the optimal modulation schemes and an efficient power allocation taking into account the performance of MMSE-DFE.

A. Modulation Selection

In order to provide specific design rules, we give recommendations for selection of a modulation scheme and symbol rate according to the performance requirements. For a given target symbol error rate ($\mathrm{SER}_{\mathrm{tgt}}$) and an unbiased signal-to-noise ratio (SNR) at the output of the MMSE-DFE equalizer $\mathrm{SNR}_{\mathrm{MMSE-DFE}}$, the constellation size M of the modulation scheme under a given performance constraint can be determined using equations from [20], resulting in

$$\begin{aligned}
&\mathrm{SER}_{\mathrm{tgt}} \geq Q(\sqrt{2\mathrm{SNR}_{\mathrm{MMSE-DFE}} \cdot \gamma_c}), && \text{(BPSK)}\\
&\mathrm{SER}_{\mathrm{tgt}} \geq 2Q(\sqrt{\mathrm{SNR}_{\mathrm{MMSE-DFE}} \cdot \gamma_c}), && \text{(4-QAM)}\\
&\mathrm{SER}_{\mathrm{tgt}} \geq \frac{4(\sqrt{M}-1)}{\sqrt{M}} Q\left(\sqrt{\frac{3\mathrm{SNR}_{\mathrm{MMSE-DFE}} \cdot \gamma_c}{M-1}}\right), && \text{(rectangular M-QAM)}\\
&\mathrm{SER}_{\mathrm{tgt}} \geq 4Q\left(\sqrt{\frac{3\mathrm{SNR}_{\mathrm{MMSE-DFE}} \cdot \gamma_c}{M-1}}\right), && \text{(non-rectangular M-QAM),}
\end{aligned} \tag{13}$$

where $Q(\cdot)$ denotes the complementary Gaussian error integral and γ_c is the nominal coding gain of an employed channel code with respect to the uncoded transmission. In order to design a coded transmission, a proper coding scheme has to be chosen. However, this issue is beyond the scope of this work. Therefore, we focus on modulation schemes and realistic signal filter design for uncoded transmission, which offers a good basis for future investigations of coded transmission for THz systems. When applying the above equations, we select the maximum M for which the SER has a value less than or equal to $\mathrm{SER}_{\mathrm{tgt}}$. Unfortunately, when this strategy for selection of the modulation scheme with maximum rate fulfilling the constraint is applied to the entire THz band no modulation scheme can be found that achieves a target symbol error rate of 10^{-3} ($\mathrm{SER}_{\mathrm{tgt}} = 10^{-3}$) or below, at an output power of 1 W (current state of the art for the output power in the THz band [9]). This is a consequence of the too low spectral signal-to-noise ratio over the entire bandwidth. Moreover, the discrete channel impulse response is very long (up to 65000 taps), see Fig. 2c). In particular, if an MMSE-DFE equalization scheme is applied after the WMF, the feedback filter of the DFE needs to have at least the length of the channel for a good performance. However, a filter with 65000 taps is not realistic. Therefore, in the following, we propose an approach based on multiple orthogonal sub-bands, which is supposed to improve the performance by reducing the frequency selectivity and thus the system complexity.

B. N-band Approach

We utilize a frequency-division based scheme by subdividing the total THz band into N sub-bands, each of equal width $B_{\mathrm{sub}} = \frac{B}{N}$, which are processed independently at the transmitter and the receiver of a single link. Here, a WMF is applied at the receiver side for each sub-band which contains an RRC filter as part of the analogue matched filter. Thus, we obtain N discrete-time channel impulse responses, denoted by $h_n[k]$, where $n \in \{1, \ldots, N\}$ represents the index of the sub-band. In order to optimize the performance of the THz link, while keeping the complexity low, the number of sub-bands must be chosen such that it provides the best trade-off between the overall achievable data rate and the implementation cost. This strategy enables a practical realization of a system, in which transmission over the whole THz band at a total output power P_{total} of 1 W is possible, as it will be discussed in detail in the following subsection. Furthermore, the N-band approach relaxes the requirements on DACs and ADCs, which, currently, can deliver data rates up to 100 Gbps [15].

C. Joint Power Allocation and Modulation Selection for N-band Approach

Our optimization problem is formulated as

$$\begin{aligned}
\underset{P_n, M_n, \forall\, n}{\text{maximize}} \quad & \sum_{n=1}^{N} \frac{R_{c,n} \log_2 M_n}{T_{\mathrm{sub}}} \\
\text{subject to} \quad & \mathrm{SER}_n \leq \mathrm{SER}_{\mathrm{tgt}}, \forall\, n \\
& \sum_n P_n = P_{\mathrm{total}},
\end{aligned} \tag{14}$$

where $R_{c,n}$ is the code rate in the n-th sub-band, M_n is the constellation size in the n-th sub-band and $T_{\mathrm{sub}} = N \cdot T$ denotes the symbol interval used in the sub-band. We refer to SER_n

as the symbol error rate of the n-th sub-band, see (13) and P_n is the transmit power of n-th sub-band.

We propose an algorithm which makes a very good use of the limited power budget regarding the overall achievable data rate. The underlying problem is a mixed integer/continuous optimization problem, therefore, an analytical closed-form solution can hardly be obtained. However, despite being suboptimal, our proposed scheme gives promising results and reveals great potential for the implementation of THz systems.

At first, we compute $\text{SNR}_{\text{MMSE-DFE},n}$, the signal-to-noise ratio at the output of the equalizer for each sub-band n when the transmitter distributes the power uniformly over the sub-bands. Depending on the determined $\text{SNR}_{\text{MMSE-DFE},n}$, we can calculate the channel quality in each sub-band after equalization and allocate the power per sub-band based on the waterfilling principle [21]. Considering the optimal waterfilling power allocation for the sub-bands P_n^*, we recompute the MMSE-DFE signal-to-noise ratio in each sub-band and denote it by $\text{SNR}^*_{\text{MMSE-DFE},n}$ for the n-th sub-band.

The power distribution is not strictly optimal anymore, since we consider finite-alphabet inputs. Therefore, in the next step Algorithm 1 is run, which receives as input parameters, P_n^* and $\text{SNR}^*_{\text{MMSE-DFE},n}$, and outputs the modulation orders M_n^* and the final powers P_n^*. The idea of the algorithm is to redistribute the initial power selection P_n^* over the sub-bands such that the SER constraint of (14) is fulfilled with equality, as described in detail in the following.

Once the $\text{SNR}^*_{\text{MMSE-DFE,n}}$ has been computed, we select the initial modulation schemes for the sub-bands according to the performance requirements (13). In other words, we will select the maximum M_n^*, for which the SER_n has a value less than or equal to the target SER. Since $\text{SER}_n \leq \text{SER}_{\text{tgt}}$ holds, the power in each sub-band P_n^* can be reduced until the current SER reaches the target SER and the constraint is fulfilled with equality. We denote the new reduced transmit power as $P^*_{\text{reduced},n}$. In this way, the extra remaining power is then collected from all sub-bands and the sum of extra powers is stored in the available power budget P_{extra}. Further on, P_{extra} is distributed iteratively among the sub-bands, adopting an auction-based approach. We denote by μ the number of the current iteration and consider P_{extra} as the extra power budget at $\mu = 0$, $P_{\text{extra}} = P^{\mu=0}_{\text{extra}}$. In each iteration μ, we define $P^{\mu}_{\text{required},n}$ as the minimum power needed to increase the modulation order in sub-band n to the next higher one under the constraint $\text{SER}_n = \text{SER}_{\text{tgt}}$. We pick the most "power efficient" sub-band, which requires less extra power for achieving a higher modulation order, i.e., $n^{*,\mu} = \arg\min_n P^{\mu}_{\text{required},n}$. This means, that sub-band is selected which offers ("bids") a most efficient usage of the available extra powers. Correspondingly, the extra allocated power to the selected band $n^{*,\mu}$ is $P^{\mu}_{\text{required},n^*}$. This power is then subtracted from the remaining power budget P^{μ}_{extra}. The power and modulation order of the selected sub-band $n^{*,\mu}$ are increased.

This procedure is iterated until there is not enough power left to further increase the constellation size in any of the sub-bands without violating the SER constraint. The remaining power is then equally distributed over all sub-bands in order to reduce SER_n and further improve the performance.

Algorithm 1 Sum rate maximization with efficient power allocation for THz systems

Input: P_n^*, $\text{SNR}^*_{\text{MMSE-DFE},n}$, SER_{tgt}, N
Output: M_n^*, P_n^*
initialize: $\text{stop\_algorithm} \leftarrow 0$, $P_{\text{extra}} \leftarrow 0$, $\mu \leftarrow 0$
for all n **do**
  using (13) find M_n^* s.t. $\text{SER}_n \leq \text{SER}_{\text{tgt}}$
  reduce P_n^* until $\text{SER}_n = \text{SER}_{\text{tgt}} \Rightarrow P^*_{\text{reduced},n}$ (new transmit power)
  $P_{\text{extra}} \leftarrow P_{\text{extra}} + (P_n^* - P^*_{\text{reduced},n})$
end for
while $\text{stop\_algorithm} \neq 1$ **do**
  $\mu \leftarrow \mu + 1$
  for all n **do**
    determine $P^{\mu}_{\text{required},n}$ to increase M_n^*
  end for
  $n^{*,\mu} \leftarrow \arg\min_n P^{\mu}_{\text{required},n} \Rightarrow P^{\mu}_{\text{required},n^*}$ (extra allocated power)
  $P^{\mu}_{\text{extra}} \leftarrow P^{\mu}_{\text{extra}} - P^{\mu}_{\text{required},n^*}$
  if $P^{\mu}_{\text{extra}} > 0$ **then**
    $M^{*,\mu}_{n^*} \leftarrow M^{*,\mu}_{n^*} \cdot 2$ (constellation size increased)
    $P^{*,\mu}_{n^*} \leftarrow P^{*,\mu}_{n^*} + P^{\mu}_{\text{required},n^*}$
  else
    for all n **do**
      $P^{*,\mu}_{n} \leftarrow P^{*,\mu}_{n} + \frac{P^{\mu-1}_{\text{extra}}}{N}$
    end for
    $\text{stop\_algorithm} = 1$
  end if
end while

IV. Numerical Results

In this section, we discuss numerical results for the achievable data rates and the modulation order. In our simulations, we assume a total transmit power of $P_{\text{total}} = 1$ W. The roll-off factor of the employed RRC transmit filter is 0.25. Also, we consider FIR filters with limited complexity, i.e., maximum of few hundred taps. The number of considered sub-bands is $N \in \{8, 16, 32\}$. We refer to the simulation scenario in Fig. 1 with the TX in the corner of the room and three different RX positions at RX_1 = (0.25 m, 2.25 m 1.5 m), RX_2 = (1.75 m, 0.5 m 1.5 m) and RX_3 = (4.5 m, 1 m 1.5 m), corresponding to a distance between the TX and the RX of 0.25 m, 2.5 m and 4.5 m, respectively. For these given transmission distances we investigate the achievable data rates with different target symbol error rate requirements. According to Fig. 3), a high data rate can be obtained by using the proposed scheme, especially for a high target SER. For a relatively small distance of d = 0.25 m, transmission is possible for all considered target symbol error

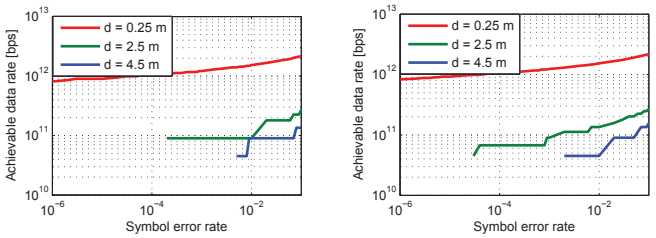

(a) $N = 16$ sub-bands (b) $N = 32$ sub-bands

Figure 3: Achievable data rates vs. target symbol error rate.

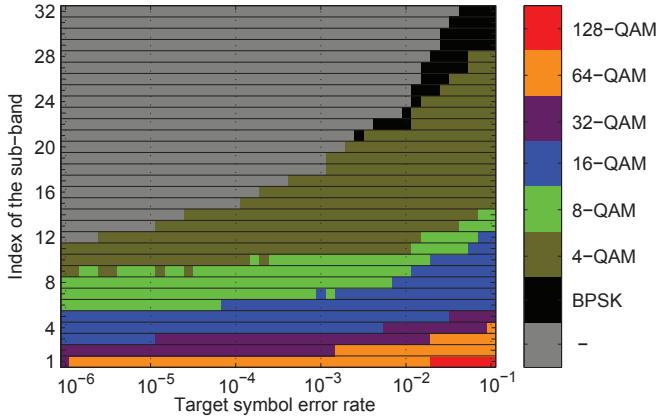

Figure 4: Proposed modulation schemes, N = 32 sub-bands, d = 0.25 m.

rates. Moreover, data rates in the order of Tbps can be attained, even for $\mathrm{SER} = 10^{-6}$. However, increasing the transmission distance would dramatically affect the achievable data rate under the symbol error rate constraint. For instance, if the TX and RX are located 4.5 m far away from each other, no transmission is possible for $\mathrm{SER}_{\mathrm{tgt}} \leq 5 \cdot 10^{-3}$ as observed in Fig. 3a). With increasing number of sub-bands, the performance improves, allowing for more robust transmissions, see Fig. 3b). In this context, it is of interest which modulation schemes should be chosen in each sub-band for an uncoded transmission in order to guarantee the $\mathrm{SER}_{\mathrm{tgt}}$ constraint. We observe from Fig. 4, that a large diversity of modulation schemes, varying between BPSK and 128-QAM is selected by Algorithm 1. Interestingly, higher order modulation schemes are selected for the lower sub-bands, while low order modulation schemes are preferred in the higher sub-bands. This can be explained according to the magnitude response of the overall channel, which is larger in the lower frequency band as compared to the higher band (-80 dB and -100 dB, respectively), see Fig. 2a). Although higher order modulation schemes beyond 16-QAM can be hardly realized with current available technologies, the continuous development of THz systems is envisioned to support higher order modulation schemes [1]. In Fig. 5, we depict the overall achievable data rate for an averaging over the positions in the room for which the TX and RX have the same distance, for two different target symbol error rates, $\mathrm{SER} = 10^{-3}$ and $\mathrm{SER} = 10^{-6}$, respectively. Losses in achievable data rate are observed, if a finite impulse response

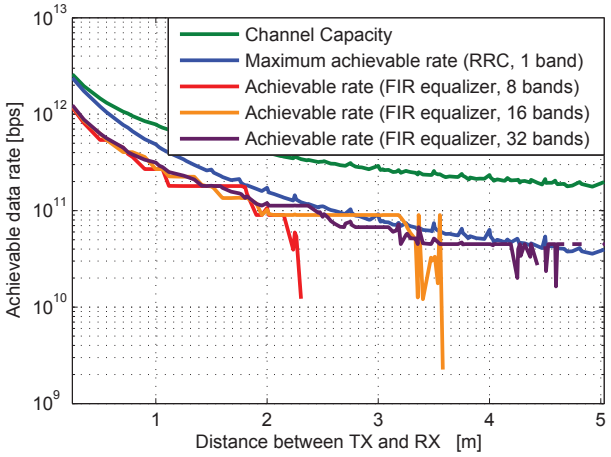

(a) $\mathrm{SER} = 10^{-3}$

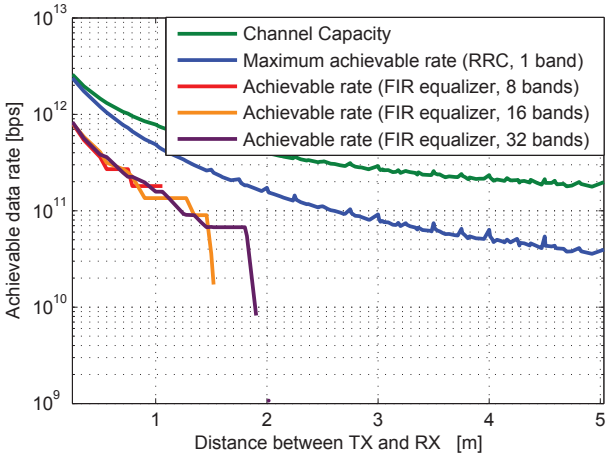

(b) $\mathrm{SER} = 10^{-6}$

Figure 5: Achievable data rates.

(FIR) equalizer and uncoded transmission is used compared to the theoretical upper bound for achievable rate for RRC filtering in conjunction with channel coding, losses which are even larger for $\mathrm{SER}_{\mathrm{tgt}} = 10^{-6}$. Moreover, a significant difference in performance can be noticed between the two cases. For $\mathrm{SER}_{\mathrm{tgt}} = 10^{-3}$ and $N = 32$, the proposed scheme allows for transmission over the entire THz bandwidth and achieves up to 75% of the theoretical limit of coded single-band transmission. For comparison, we also show the channel capacity. The proposed solution performs $\approx 50\%$ and $\approx 80\%$ worse than the channel capacity for small distances and large distances, respectively, leaving a noticeable gap for the code design. However, setting $\mathrm{SER} = 10^{-6}$ dramatically reduces the performance of the system. According to Fig. 5b), uncoded transmission is not possible beyond a distance of 2 m. Related investigations on the transmission distance have been conducted in [14] for multi-carrier systems. It should be noted that for short distances (e.g. 0.25 m) the channel averaging can be done over much more positions than for higher distances (e.g. 5 m). This provides a better accuracy for smaller transmission distances, which is reflected in the smoothness of the curves.

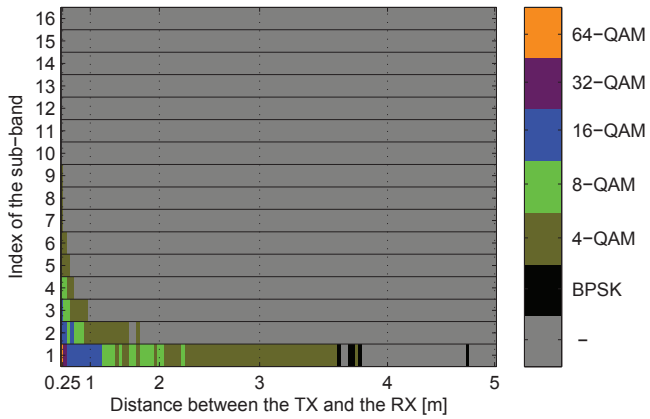

Figure 6: Proposed modulation schemes, N = 16 sub-bands, $\mathrm{SER} = 10^{-3}$.

Finally, in Fig. 6, we present our recommendation on the selection of the modulation schemes for the different sub-bands for variable distances between the TX and the RX. Here, we set $\mathrm{SER}_{\mathrm{tgt}} = 10^{-3}$. Moreover, for every considered distance in the room that does not correspond to a unique TX/RX pair instead of averaging, we always pick the modulation schemes corresponding to the highest data rate. It can be noticed that the modulation order decreases non-monotonically due to the specific position of the TX/RX in the room for increasing transmission distances.

The obtained results indicate the limitation of THz wireless communication systems to short-link indoor applications. This restriction might, however, be overcome by the realization of a massive multiple-input multiple-output (MIMO) system in the THz band [22]. The proposed N-band approach could be also extended to realize a multi-user system with users occupying one or more sub-bands each.

V. Conclusions

In this paper, we have considered the design of uncoded point-to-point THz transmission systems using realistic transmit, receive, and equalization filters. We have addressed the problem of equalizing a very long dispersive channel impulse response by utilizing a frequency-division based scheme with multiple sub-bands. We have shown an approach to maximize the achievable data rates by employing an iterative power allocation algorithm. In addition, recommendations for the modulation scheme for a given distance and target symbol error rate for maximizing the achievable data rate have been given. In this context, our investigations revealed a possibility of indoor communication with high data rates in the order of Tbps under realistic error rate constraints. Moreover, the sub-band approach offers a good basis for future investigations of coded transmission for THz systems. Hence, this work provides a fundamental background for future enhancements like multi-user communication and spatial diversity.

References

[1] H. Song and T. Nagatsuma, "Present and future of terahertz communications", *IEEE Transactions on Terahertz Science and Technology*, vol. 1, no. 1, pp. 256–263, 2011.

[2] S. Cherry, "Edholm's law of bandwidth", *IEEE Spectrum*, vol. 58-60, 2004.

[3] IEEE-802.15-WPAN, "Terahertz Interest Group (IGthz)", 2014. [Online]. Available: http://www.ieee802.org/15/pub/IGthzOLD.html.

[4] J. Federici and L. Moeller, "Review of Terahertz and subterahertz wireless communications", *Journal of Applied Physics*, vol. 107, p. 111 101, 2010.

[5] L. Moeller, K. Su, R. Barat, and J. F. Federici, "THz and IR signaling through fog scintillations", *European Wireless (EW), 2012. EW. 18th European Wireless Conference*, pp. 1–5, 2012.

[6] J. F. Federici and J. Ma, "Comparison of Terahertz versus infrared free-space communications under identical weather conditions", *Proc. of the 39th International Conference on Infrared, Millimeter, and Terahertz waves (IRMMW-THz)*, 2014.

[7] D. Saeedkia, *Handbook of Terahertz technology for imaging, sensing and communications*. Woodhead Publishing Limited, 2013.

[8] Y. Hao, L.-A. Yang, and J.-C. Zhang, "Gan-based semiconductor devices for Terahertz technology", *Terahertz Science and Technology*, vol. 1, no. 2, 2008.

[9] L. Li, A. Valavanis, J. Zhu, J. Freeman, L. Chen, A. Davies, E. Linfield, and P. Dean, "Terahertz quantum cascade lasers with >1 W output powers", *Electronics Letters*, vol. 50, no. 4, pp. 309–311, 2014.

[10] T. Nagatsuma, K. Kato, and J. Hesler, "Enabling technologies for real-time 50-Gbit/s wireless transmission at 300 GHz", *Proc. of the Second Annual International Conference on Nanoscale Computing and Communication - NANOCOM*, 2015.

[11] A. Moldovan, M. A. Ruder, I. F. Akyildiz, and W. H. Gerstacker, "LOS and NLOS channel modeling for Terahertz wireless communication with scattered rays", *Proc. of the IEEE Globecom Emerging Technologies for 5G Wireless Cellular Netwroks Workshop*, pp. 388–392, 2014.

[12] J. Jornet and I. Akyildiz, "Channel modeling and capacity analysis for electromagnetic wireless nanonetworks in the terahertz band", *IEEE Transactions on Wireless Communications,*, vol. 10, no. 10, pp. 3211–3221, 2011.

[13] J. M. Jornet and I. F. Akyildiz, "Femtosecond-long pulse-based modulation for Terahertz band communication in nanonetworks", *IEEE Transactions on Communications*, vol. 62, no. 5, pp. 1742–1754, 2014.

[14] C. Han and I. F. Akyildiz, "Distance-aware multi-carrier DAMC modulation in Terahertz band communication", *Proc. of the IEEE International Conference on Communications (ICC)*, 2014.

[15] C. Laperle and M. OSullivan, "Advances in high-speed DACs, ADCs, and DSP for optical coherent transceivers", *Journal of Lightwave Technology*, vol. 32, no. 4, pp. 629–643, 2014.

[16] R. Piesiewicz, C. Jansen, S. Wietzke, D. Mittleman, M. Koch, and T. Kürner, "Properties of building and plastic materials in the THz range", *International Journal of Infrared and Millimeter Waves*, vol. 28, no. 5, pp. 363–371, 2007.

[17] I. Llatser, A. Cabellos-Aparicio, E. Alarcon, J. M. Jornet, A. Mestres, H. Lee, and J. Sole-Pareta, "Scalability of the channel capacity in graphene-enabled wireless communications to the nanoscale", *IEEE Transactions on Communications*, vol. 63, pp. 324–333, 2014.

[18] L. Kish, "Stealth communication: Zero-power classical communication, zero-quantum quantum communication and environmental-noise communication", *Applied Physics Letters*, vol. 87, no. 23, p. 234 109, 2005.

[19] J. Cioffi, G. Dudevoir, M. Vedat Eyuboglu, and G. Forney, "MMSE decision-feedback equalizers and coding. i. equalization results", *IEEE Trans. Commun.*, vol. 43, no. 10, pp. 2582–2594, 1995.

[20] J. G. Proakis and M. Salehi, *Digital Communications*. McGraw-Hill Education, 2007.

[21] D. Tse, *Fundamentals of wireless communication*. Cambridge university press, 2005.

[22] I. Akyildiz, J. Jornet, and C. Han, "Terahertz band: Next frontier for wireless communications", *Physical Communication*, vol. 12, pp. 16–32, 2014.